Magnetic-field-dependent thermodynamics of Mn_{12}-acetate single crystals at low temperatures

F. Fominaya,* J. Villain, T. Fournier, P. Gandit, and J. Chaussy
CRTBT-CNRS, 25 avenue des Martyrs, Boîte Postale 166, F-38042 Grenoble, France

A. Fort
Department of Physics, University of Florence and Istituto Nazionale di Fisica della Materia di Firenze, Largo E. Fermi 2, I-50125 Firenze, Italy

A. Caneschi
Department of Chemistry, University of Florence, Via Maragliano 77, 550144 Firenze, Italy
(Received 16 January 1998; revised manuscript received 11 May 1998)

Thermal measurements of single microcrystals of Mn_{12} acetate have been performed with a particularly sensitive nanocalorimeter. Heat-capacity measurements as a function of applied magnetic field demonstrate magnetization quantum tunneling at the crossing of crystal-field levels. We present a theoretical model of the magnetic heat capacity of Mn_{12} acetate that approximately agrees with experimental results. Temperature measurements as a function of a slowly scanned magnetic field confirm earlier magnetization measurements and suggest that the thermal coupling between bath and sample, as well as the thermal conductivity of the crystals, play a major role in the magnetization reversal. [S0163-1829(98)06041-X]

I. INTRODUCTION

There has been intensive recent study of magnetization reversal against a high anisotropy barrier by macroscopic quantum tunneling in very small monodomain particles.[1] Below a certain crossover temperature, the relaxation of magnetization in these mesoscopic particles is much faster than predicted by the classical models of magnetization reversal, such as the Néel-Brown model.[2] A great effort is underway to determine whether this effect is due to quantum tunneling of magnetization because of both theoretical interest and future technical applications of nanomagnets.[3] The investigator of mesoscopic magnetic systems encounters the difficulty of clearly discerning quantum-mechanical effects from classical ones. Real samples very often consist of a set of particles that unavoidably have different shapes and sizes, so that the distribution of the relevant parameters, such as anisotropy constant and particle volume, is relatively broad and makes the interpretation difficult. In addition, an exchange coupling between particles is often unavoidable. Therefore measurements are preferably made on either a single particle,[4] which presents an experimental challenge due to the smallness of the sample, or on one of the few known systems of identical, noninteracting particles. Mn_{12}-acetate crystals[5] (for a short review, see Ref. 6) belong to the latter class as they are arrangements of identical magnetic clusters in an organic matrix, without exchange coupling from one cluster to another. Each cluster is composed of 12 manganese ions that are coupled in a ferrimagnetical configuration to a $S=10$ macrospin (henceforth we will refer to it simply as ''spin''). Excitations within the cluster can be neglected at temperatures sufficiently far below[7] 30 K. The crystals are rectangular parallelepipeds with tetragonal symmetry. A strong crystalline anisotropy lifts the $2S+1$ degeneracy of the magnetic levels in zero field, creating a configuration where two wells are separated by a barrier[8] of about 60 K. The relaxation time of the magnetization is therefore very long at low temperatures.[9] The spacing between the levels in the wells is large (up to about 12 K) and thus typical of a microscopic, quantum system. A resonant tunneling of molecular spins between matching levels on opposite sides of the potential barrier formed by the anisotropy was recently demonstrated.[10–13]

The manganese system is superparamagnetic and can be described by a Hamiltonian of the form[14]

$$\mathcal{H}=-D\mathbf{S}_z^2-g\mu_B\mathbf{S}_z\mathbf{H}+\mathcal{H}^l, \tag{1}$$

where $D=0.6$ K is the anisotropy energy per cluster, $DS_z^2=60$ K is the anisotropy energy, $\mathbf{H}$ the magnetic field applied parallel to the easy axis of magnetization, $g\simeq 2$ is the gyromagnetic factor, and S_z the spin per cluster. The term $\mathcal{H}^l$ is a Hamiltonian that does not commute with S_z and results from the demagnetizing field, dipole coupling, higher anisotropy terms, and/or hyperfine splitting. A great effort is underway to understand its origin,[15,2,14] as it rules the tunneling phenomenon and is the key to an enhancement of the relaxation time that would be necessary for technical applications.

Up to now the Mn_{12} complex has been studied by magnetization measurements, ac susceptibility, and electron paramagnetic resonance measurements (see, for example, Refs. 9, 12, 16, and 17). The heat capacity has been measured on powder samples of Mn_{12} acetate.[11] These studies show that the environment acts on the quantum tunneling of magnetization, thermally activating the tunneling between levels in a way that is still not well understood. For these reasons it is important to study the interaction of the magnetic system of the crystal with the phonon bath.

Small single crystals generally have a better structural quality than big ones, while the broadening found on powder samples due to the slightly different characteristics of each

crystal or to their orientation dispersion in an applied magnetic field is absent. On the other hand, the thermal conductivity of Mn_{12} acetate is very low in the usually studied range of temperatures (0.5–30 K), so that small crystals reach thermal equilibrium more rapidly than larger ones, and therefore are better suited for accurate dynamic thermal measurements. A very sensitive nanocalorimeter, especially devised for such measurements,[18] allowed us to perform unprecedented specific-heat measurements of small Mn_{12}-acetate single crystals.[13] In this article, we first describe the theoretical backgrounds to specific-heat measurements of slowly relaxing modes in a magnetic double-well system. Then we compare the theoretical predictions to the measured specific heat $C(H)$ of small single crystals of Mn_{12} acetate as a function of an applied magnetic field H at different temperatures and frequencies. Finally, we study the temperature $T(H)$ of the crystals as a function of a scanning magnetic field and we suggest a qualitative interpretation of the results.

II. SPECIFIC HEAT OF SLOWLY RELAXING MODES

The *conditio sine qua non* to measure a specific heat in thermal equilibrium is that any internal relaxation process of the sample be much shorter or much longer than the measuring time. In the first case all relaxation processes have time to take place, and a thermal equilibrium measurement can be performed. In the second case, the slow relaxation modes are ignored and all degrees of freedom except those which depend on the slow modes are measured.

In certain cases, as for instance the heat-capacity measurements performed in the late 1970s on vitreous silica and other metastable systems (Ref. 19 and references therein) or in our present measurements of Mn_{12}-acetate, there is a mode with a relaxation time comparable to the measuring time, so that the measured magnitude cannot be considered any more an equilibrium specific heat, but rather a kind of linear ''susceptibility.'' This linear susceptibility represents a frequency-dependent specific heat $C(\omega)$, if we admit that the inverse of the measuring time defines a frequency $\omega/(2\pi)$. Note that the measurement is nevertheless in equilibrium with regard to the average temperature and the magnetic field. As pointed out by Birge and Nagel,[20] frequency-dependent specific-heat data have a unique feature. The specific heat is linked to the thermodynamics of the system and therefore couples not only to magnetic, electric, or structural changes, but to all modes of the system. This is not true for dielectric, magnetic, or mechanical susceptibilities, so, in some cases, specific heat might be the only useful analysis tool.

In this section we show how to deal with nonequilibrium specific-heat data and how to get valid microscopic information from the measurement of heat capacity by means of the ac steady-state method[21] of a magnetic double-well system. We proceed in the following way. First, we define a frequency-dependent specific heat $C(\omega)$ according to linear response theory. Then the dynamics of spins in the double well is studied as a function of the relaxation time τ of the system and the frequency ω of the heat-capacity measurement. We obtain a formula [formula (24)] that relates the measured specific heat $C(\omega)$ to ω, τ, C_{bi}, and C_{uni}, where $C_{bi}=C(\tau\rightarrow 0)$ and $C_{uni}=C(\tau\rightarrow\infty)$ are the two limiting equilibrium values discussed above. Finally, we use the obtained formulas to study the example of a double-well system: Mn_{12}-acetate crystals.

A. The general case for ac steady-state measurements

The temperature modulation induced in the ac steady-state method is a sum of Fourier components. Linear response theory will be assumed to hold, so that the effect of the various Fourier components is additive and is sufficient to consider a single Fourier component. The temperature of the sample is then

$$T(t)=T_0+\delta T(t), \tag{2}$$

where

$$\delta T(t)=\delta T_0\cos(\omega t). \tag{3}$$

Within linear response theory, formula (3) implies that the power $\mathcal{P}(t)$ transferred to the sample from the external world is also a sinusoidal function of time, which depends on a phase shift φ, namely,

$$\mathcal{P}(t)=-\delta\mathcal{P}_0\sin(\omega t-\varphi). \tag{4}$$

We shall now see how a frequency-dependent specific heat can be defined and deduced from the two measured quantities $\mathcal{P}(t)$ and $\delta T(t)$. We shall generally assume that the measurement is performed at constant sample volume and more generally ''without external work.'' [22] In such conditions, *at thermal equilibrium*, the heat capacity MC (where M is the sample mass and C the specific heat) is usually defined as the ratio $\delta U/\delta T$ of the increase δU of the energy of the sample to the temperature increase δT in a transformation where the sample is at equilibrium. In the nonequilibrium measurement of interest, the energy $U(t)$ of the sample at time t is, within linear response theory, a sinusoidal function of time, namely,

$$U(t)=U_0+\delta U(t), \tag{5}$$

where the relation $\mathcal{P}(t)=dU(t)/dt$ implies

$$\delta U(t)=\delta U_0\cos(\omega t-\varphi) \tag{6}$$

with

$$\delta U_0=\delta\mathcal{P}_0/\omega. \tag{7}$$

Following the usual definition of susceptibilities in linear response theory, a frequency-dependent heat capacity $MC(\omega)$ can be defined as

$$MC(\omega)=\frac{U_\omega}{T_\omega}, \tag{8}$$

where we introduced the Fourier coefficients

$$T_\omega=\frac{1}{2\pi}\int_0^{2\pi}dt\,\delta T(t)\exp(-i\omega t)=\delta T_0/2 \tag{9}$$

and

$$U_\omega=\frac{1}{2\pi}\int_0^{2\pi}dt\,\delta U(t)\exp(-i\omega t)=(\delta U_0/2)\exp(i\varphi). \tag{10}$$

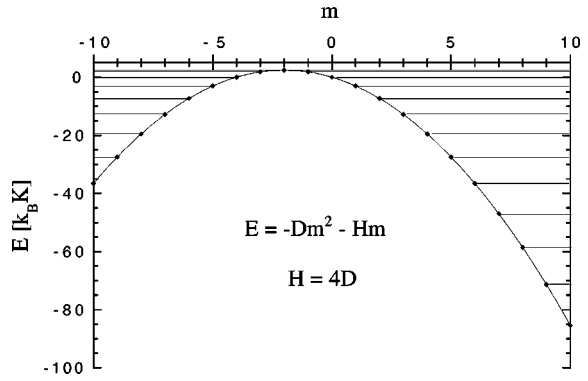

FIG. 1. Double-well system for a spin $S=10$ at a magnetic field of $H=4D$.

One can deduce the ''absolute frequency-dependent heat capacity''

$$M|C(\omega)|=\frac{\delta U_0}{\delta T_0}, \tag{11}$$

which is the absolute value of $MC(\omega)$. Even though the phase shift φ does not appear in Eqs. (11) and (7), it should be introduced in order to relate the specific heat to a microscopic model, which is the task of the next section.

B. $C(\omega)$ in a double-well potential

We shall now consider the particular case of a system where a potential barrier separates the physical states into two sets or ''wells'' such that thermal equilibrium is rapidly established inside each well while, at low temperature, thermal equilibrium between the two wells is established only after a long time τ. Examples of such systems are given by big magnetic molecules like Mn_{12}, as described in the Introduction. In reality, the double-well system is a microscopic element of a macroscopic set of many double wells, but in the following we shall only consider a single double well called ''the system.'' The interaction with the rest of the sample is represented only by the relaxation time τ. The two wells will be designated by the signs ''+'' and ''−.'' The system has a probability $p^+(t)$ to be in the + well at time t, and a probability $p^-(t)$ to be in the − well. Of course, $p^+(t)+p^-(t)=1$. As can be seen in Fig. 1 a state $m>0$ can pass from the + well to the − well at a high magnetic field. Thus it is appropriate to introduce a function ψ_m which is, at least approximately, equal to 1 if the state $|m\rangle$ belongs to the + well and to −1 if the state $|m\rangle$ belongs to the − well. It follows that the function $(1+\psi_m)/2$ is equal to 1 if the state $|m\rangle$ belongs to the + well and to 0 if the state $|m\rangle$ belongs to the − well, while the function $(1-\psi_m)/2$ is equal to 0 if the state $|m\rangle$ belongs to the + well and to 1 if the state $|m\rangle$ belongs to the − well.

In our numerical calculations we assumed

$$\psi_m=m/|m| \quad (m\neq 0), \quad \psi_0=0. \tag{12}$$

This definition is only correct in zero field, but can be used also for a nonvanishing field if the temperature is so low that the population of states $|m\rangle$ is negligible for small m. One should have

$$\sum_m p_m(t)(1\pm\psi_m)/2=p^{\pm}(t). \tag{13}$$

Moreover, thermal equilibrium inside each well implies that the probability $p_m(t)$ that the system is in state $|m\rangle$ at time t satisfies the relation $p_m(t)/p_n(t)=\exp[-\beta(E_m-E_n)]$ for any pair of states $|m\rangle$ and $|n\rangle$ belonging to the same well. It follows

$$p_m(t)=\left[\frac{1+\psi_m}{2}\frac{p^+(t)}{z^+}+\frac{1-\psi_m}{2}\frac{p^-(t)}{z^-}\right]\exp(-\beta E_m), \tag{14}$$

where

$$z^{\pm}(t)=\sum_m \exp(-\beta E_m)\,\frac{1\pm\psi_m}{2}. \tag{15}$$

Our aim is to calculate the specific heat through formula (8), where M is the mass of the system and U_ω is the Fourier transform of the energy of the system at time t,

$$U(t)=\sum_{-s}^{s} p_m(t)E_m. \tag{16}$$

The next task is the determination of $p^+(t)$ [and, in the same way, $p^-(t)$]. At thermal equilibrium this probability would be

$$p^+_{eq}=\frac{\sum_m \exp(-\beta E_m)(1+\psi_m)/2}{\sum_m \exp(-\beta E_m)}=\frac{z^+}{z}, \tag{17}$$

where

$$z=z^++z^-. \tag{18}$$

At any time t, the sample has a certain temperature $T(t)$ given by Eqs. (2) and (3); expression (17) has therefore a well-defined value and $p^+(t)$ tends to get closer to that value. In the simplest cases one can assume a linear relation, namely,

$$\frac{\partial}{\partial t}p^+(t)=-\frac{1}{\tau}[p^+(t)-p^+_{eq}], \tag{19}$$

where τ is the relaxation time already introduced, and p^+_T depends on time through the temperature T. Let us consider the simple case where the jump rate is very low. Then the probability $p^+(t)$ to be in the + well is almost independent of t and equal to its average value p^+_0. When, for instance, the temperature is stationary (i.e., maximum or minimum), the flow of energy from one well to the other is maximum according to Eq. (19), so that the energy has no reason to be stationary and therefore there must be a phase shift φ. As will be seen later, φ vanishes in the absence of jumps between wells.

For a weak temperature modulation, Eq. (19) can be linearized and its solution is

$$p^+(t)=p_0^+ + \frac{\delta p_0^+}{\sqrt{1+\omega^2\tau^2}}\cos(\omega t-\alpha), \tag{20}$$

where

$$\tan\ \alpha=\omega\tau \tag{21}$$

and

$$p_0^+=\frac{\sum_m \exp(-\beta_0 E_m)(1+\psi_m)/2}{\sum_m \exp(-\beta_0 E_m)}, \tag{22}$$

is the probability to be in the + well at $T=T_0$. The expression of δp_0^+ is given in the Appendix.

Inserting Eq. (20) into Eq. (16) one obtains after some calculations given in the Appendix

$$\delta U(t)=|C(\omega)|\,\delta T_0\cos(\omega t-\varphi), \tag{23}$$

where φ is not accessible to present experiments. Its expression is given in the Appendix. The quantity accessible is the ''absolute specific heat'' at frequency ω,

$$|C(\omega)|=\sqrt{C_{uni}^2+\frac{C_{bi}^2-C_{uni}^2}{1+\omega^2\tau^2}}, \tag{24}$$

where C_{bi} is the equilibrium or ''bilateral'' specific heat ($\tau=0$), while C_{uni} is the ''unilateral'' specific heat, i.e., the specific heat that is measured when jumps over the potential barrier are impossible during the measuring time $2\pi/\omega$ because $\tau=\infty$. Their expressions are easily obtained and given in the Appendix. The phase α given by Eq. (A9) is equal to $\pi/2$ in the unilateral limit, and to 0 in the bilateral limit. However, the phase shift φ is equal to 0 in both limits. It should be so, because both limits correspond to an equilibrium situation. The bilateral limit is the true equilibrium, and the unilateral limit is an equilibrium where one of the wells is ignored.

Eliminating α between Eqs. (21) and (24), one obtains

$$\tau=\frac{1}{\omega}\sqrt{\frac{C^2(\omega)-C_{bi}^2}{C_{uni}^2-C^2(\omega)}}, \tag{25}$$

which looks appealing since it allows the relaxation time to be determined directly from the specific heat. However, Eq. (25) should be handled with care because $C^2(\omega)$ has to be the magnetic specific heat, corrected for the phonon contribution. This correction, discussed in the next section, can be a source of errors.

The essential result of this section is formula (24), which relates the experimentally measured specific heat to the thermodynamic quantities C_{bi} and C_{uni} and to the relaxation time τ. The time τ can be compared with the results of magnetic measurements, as we will do in the next section, and can be calculated if the spin-phonon interaction is known. This calculation has been made in the case $H=0$ by Fort *et al.*[23] and in the general case by Luis *et al.*[25] The specific application to specific-heat measurements has been made by Fernández *et al.*[24] who also obtain a formula equivalent to Eq. (24) by a method different from ours.

III. HEAT-CAPACITY MEASUREMENTS OF Mn_{12}-ACETATE CRYSTALS

Our nanocalorimeter[18] basically consists of a 3-μm-thick silicon membrane suspended in vacuum and linked to the thermal bath by twelve narrow silicon bridges. A planar NbN thermometer and a CuNi heater are placed on this membrane and the samples are pasted with grease on the backside of the same. The experimental setup permits not only the study of extremely small crystals, but also a very accurate knowledge of the temperature of the sample during measurement. Every configuration of the magnetic system can be sampled by tuning an applied magnetic field. The field was varied parallel to the easy axis of magnetization, usually from -1 to 1 T. The heat capacity was measured, as described in Ref. 18, by recording the amplitude of the temperature oscillations. The phase shift φ, which could in principle also be measured, turned out to be very sensitive to parasitic capacitances and was therefore ignored.

Three different samples were measured and the same qualitative results were found in each case. The quality measurements were obtained with the smaller crystals ($30\times60\times400$ μm for 1 μg weight and $790\times180\times75$ μm^3 for 20 μg). The largest one ($1100\times480\times200$ μm^3) seemed to be less adapted for the device as, due to its size and low thermal conductivity, it did not sufficiently well follow the temperature oscillations of the measurement. The typical working frequencies ω ranged between 25 and 120 Hz.

A. Contribution of the lattice vibrations

The measured heat capacity consists of a sum of three contributions: The ''addenda'' (sample holder+grease), the magnetic heat capacity, and the lattice heat capacity. Other contributions like the hyperfine heat capacity are supposed to be negligible in the explored range of temperature. Addenda are the major source of error for an exact determination of the specific heat of the crystal: The contribution of the bare sample holder is known (4 nJ/K at 4 K) but that of the grease used to paste the sample can only be estimated. In any case, addenda usually represent less than 10% of the total heat capacity.

Since the lattice contribution is independent of the field, it can be evaluated by subtraction of the addenda contribution and the magnetic heat capacity *in zero field* from the measured heat capacity. The zero-field magnetic specific heat $C_{mag}(0)$ is calculated from formula (A13) or (A11), which yield the same result in zero field. The estimation of the volume of the sample can also introduce a small error in the latter calculation. Curve 2 shows the measured total heat capacity (lattice+magnetic) of the 20-μg sample that is compared to a calculated curve and to the values obtained by Novak *et al.*[11] The inset in Fig. 2 shows the determination of the Debye temperature to $\Theta_{Debye}=41$ K from the lattice contribution using the well-known low-temperature approximation ($T\ll\Theta$) of the Debye theory:[26]

$$C_{lat}\simeq 234 N_a k_B\left(\frac{T}{\Theta}\right)^3, \tag{26}$$

where Θ is the Debye temperature and N_a is the number of atoms of the crystal.

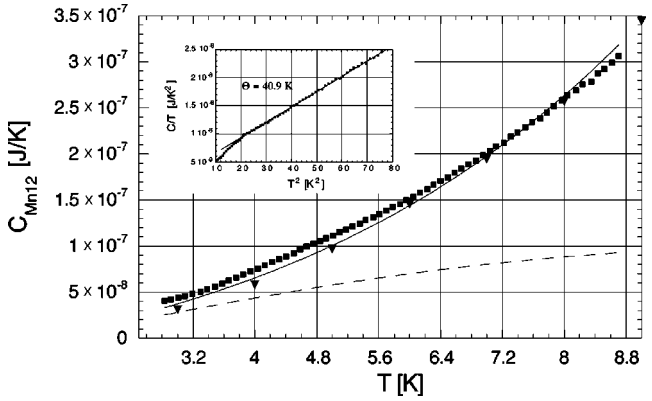

FIG. 2. Squares: Heat capacity of Mn_{12} acetate as a function of temperature, measured on the 20-μg single crystal. Triangles: Values of Novak *et al.* Continuous line: Calculated curve with $\Theta_{Debye}=38$ K (obtained by Novak *et al.*). Dashed line: Calculated curve with $\Theta_{Debye}=40.9$ K. Pointed line: Calculated magnetic heat capacity. Inset: Determination of Θ_{Debye}.

B. Heat-capacity measurements as a function of magnetic field

Each of the following curves was recorded allowing thermal equilibrium to be reached at every magnetic field step. Figure 3 shows heat-capacity curves recorded at a fixed frequency. The curves below 3.5 K have no structure. In Fig. 4 they are compared to the calculated magnetic heat capacity in the unilateral limit (the bilateral limit is also shown for comparison). At temperatures below 3 K the relaxation time τ, which roughly follows an Arrhenius law, is much longer (a few seconds) than the measuring time (tenths of ms), so, as expected, the $T=2.6$ K curve clearly approaches the unilateral limit. At those temperatures the calculated heat capacities strongly depend on the height of the anisotropy barrier. The curves shown fit best with a barrier of $\Delta E/K_B=62\pm2$ K. This value is in agreement with the usually admitted value of 61 K.[27]

For the frequency $\omega=25$ Hz, the product $\omega\tau$ is of order unity between 3.5 and 5 K. In this range of temperatures a symmetric pattern of peaks appears at magnetic field values of ±0.4 and ±0.8 T.

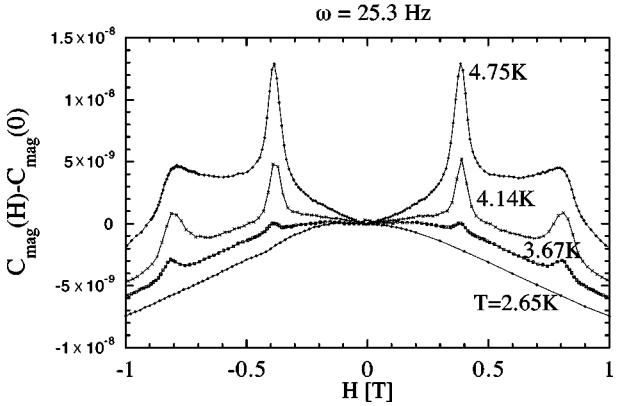

FIG. 3. Magnetic heat capacity of the 20-μg Mn_{12}-acetate monocrystal vs the applied magnetic field, measured at $\omega=25$ Hz. The zero-field-calculated magnetic heat capacity $C_{mag}(0)$ is 56.0, 47.7, 40.2, and 21.3 nJ/K for, respectively, $T=4.75$, 4.14, 3.67, and 2.65 K. The differences between the measured values $C_{total}(0)$ and the calculated $C_{mag}(0)$ are the magnetic-field-independent addenda (lattice+sample holder contribution).

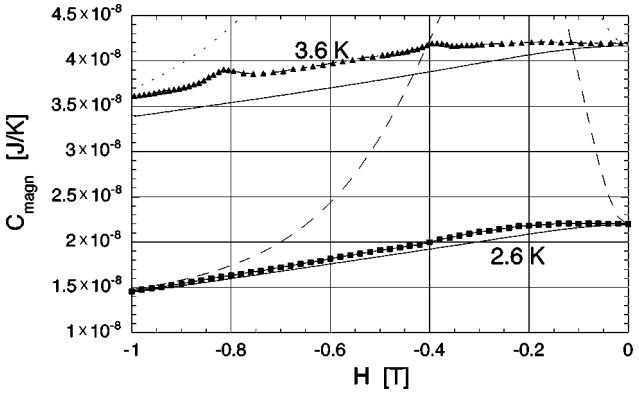

FIG. 4. Measured and calculated (continuous line: lateral limit, dashed line: bilateral limit) magnetic heat capacity of the 20-μg crystal at $T=2.6\pm0.05$ K and $T=3.65\pm0.02$ K.

Above 5 K the anomalies disappear into a broad maximum, which shifts to higher field values when the temperature is raised (see Fig. 4 of Ref. 13). This behavior is predicted by Eq. (A12). As can be seen from Fig. 5 a qualitative agreement exists between the calculated curve and measured curve. However, the measured specific heat is appreciably lower than the calculated one. Further measurements will be necessary to clarify this discrepancy. Note that, at the temperature $T=5.7$ K, which corresponds to the figure (and at higher temperatures), the values of the relaxation time τ published by Hernández *et al.*[28] (which we have used to calculate our curve) are such that $\omega\tau\ll1$, so the calculated curve is equal to the equilibrium heat capacity C_{bi}.

All the curves can be explained with the present model. To approach the unilateral ($\omega\tau\gg1$) or the bilateral regime ($\omega\tau\ll1$) either temperature or frequency can be varied. At $T=4.3$ K (Fig. 6) the system is in the intermediate regime for $\omega=18.8$ Hz and tends towards the unilateral regime for higher frequencies. As expected the peaks at $H=D$ disappear sooner than the peaks at $H=2D$. At 5.1 K (Fig. 7) the system is close to the bilateral limit for $\omega=18.8$ Hz and clearly in the intermediate regime for higher frequencies.

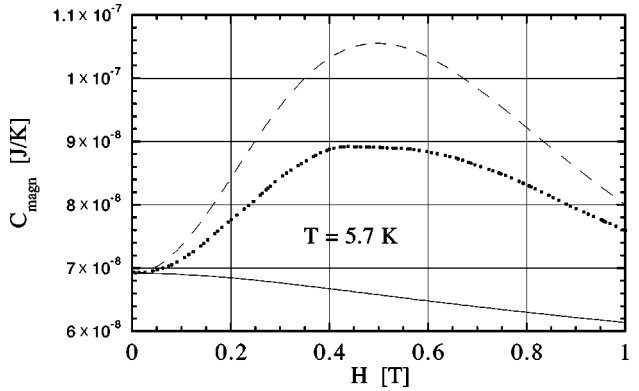

FIG. 5. Measured (squares) and calculated (dashed line) magnetic heat capacity of the 20-μg crystal at $T=5.7$ K. The theoretical curve was calculated for $\omega=25$ Hz and $\tau=2.4$ ms (Ref. 16) (it is nearly identical to C_{bi}). The height of the anisotropy is a less important fitting parameter: No substantial difference is observed between a fit $\Delta E/K_B=60$ K and a fit $\Delta E/K_B=70$ K. The flat curve is C_{uni}.

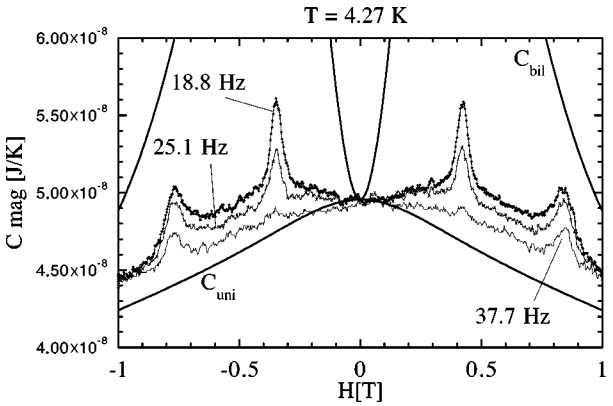

FIG. 6. Magnetic heat-capacity curves at different frequencies ω of the 20-μg crystal. The higher frequency approaches the unilateral regime.

However, the mean time τ follows an Arrhenius law of thermal activation;[27] thus temperature intervenes exponentially in $\omega\tau$ and frequency only linearly.

The higher the temperature the smaller is the magnetic contribution compared to the lattice contribution, so sensitivity is lost at higher temperatures and it is more difficult to observe the peaks. At low temperatures the experiment is limited by the minimum frequency of the lock-in amplifier (20 Hz in our case).

The peaks always appear in the range of temperatures and frequencies where $\omega\tau \simeq 1$ when the Zeeman levels of the two sides of the barrier match at discrete magnetic-field values. The sudden reduction of the relaxation time of magnetization due to a tunneling effect leads the system to pass from a state where $\omega\tau > 1$ to a state where $\omega\tau < 1$, i.e., from a rather unilateral regime to a bilateral regime.

Formula (25) allows the relaxation time to be calculated from a heat-capacity curve: Figure 8 shows the calculated τ for the 4.7-K curve of Fig. 3. A comparison of the results with the data of Figs. 3 and 4 of Hernández *et al.*[28] shows that the general shape of our curve agrees quite well with theirs; the values differ however by a factor of 3. For other temperatures and frequencies the obtained relaxation times are also more than two times longer than the expected values. A test of formula (24) is that it should be independent of

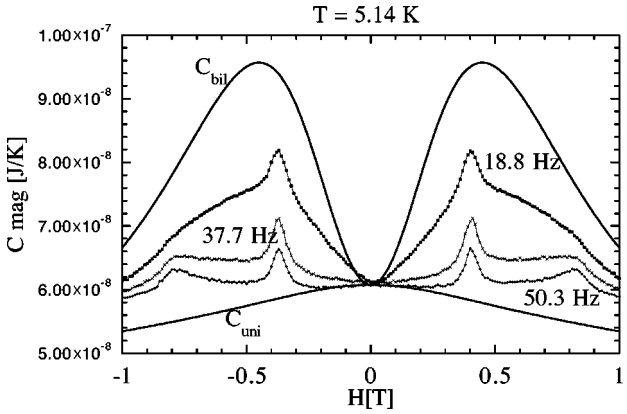

FIG. 7. Magnetic heat-capacity curves at different frequencies ω of the 20-μg crystal. The lower frequency approaches the bilateral regime.

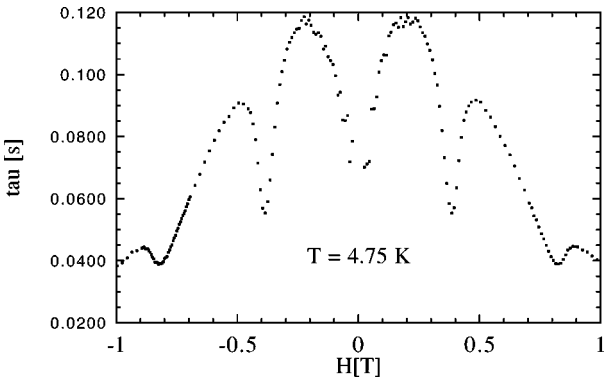

FIG. 8. Relaxation times τ as a function of magnetic field calculated from Fig. 3.

ω. In Fig. 9 $\sqrt{[C^2(\omega)-C_{bi}^2]/[C_{uni}^2-C^2(\omega)]}$ has been traced versus ω for the curves of Figs. 6 and 7. In principle, straight lines through the origin are expected. Apart from one point this is roughly the case.

C. Nonequilibrium measurements of heat capacity in a rapidly swept field

Nonequilibrium measurements mean in this case that insufficient time is given for the sample to achieve equilibrium with regard to the magnetic field, so hysteresis effects appear and a time-dependent heat capacity $C(t)$ is measured. Nonequilibrium measurements are analogous to usual magnetic hysteresis measurements.[29,12]

Our measurements were performed at rather low temperatures (typically $T < 3$ K), where the relaxation time of the magnetic system (τ) is long, by scanning the magnetic field from -1 to 1 T at a rate of 1 mT/s. The measurement was averaged over 1 s for each data point. In this way the system was prevented from reaching equilibrium. In Fig. 10, discontinuities in the $C(H)$ curve are observed. They can be interpreted within the framework of the double-well model as magnetization tunneling when magnetic levels cross at positive magnetic-field values $H_n = n \times D/(g\mu_B) \simeq n \times 0.4$ T, $n = 1,2,\ldots$. Once a spin tunnels to the spin-up well, it relaxes to the ground state with heat emission and, as the temperature is low compared to the 12 K of the first excited level, the process is irreversible. This explains why the dis-

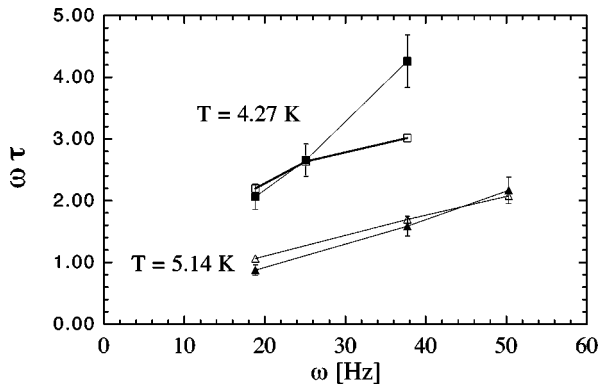

FIG. 9. Triangles: $T = 5.14$ K, squares: $T = 4.27$ K. Filled: $\omega\tau$ at $H = D$, open: $\omega\tau$ at $H = 0.7$ T.

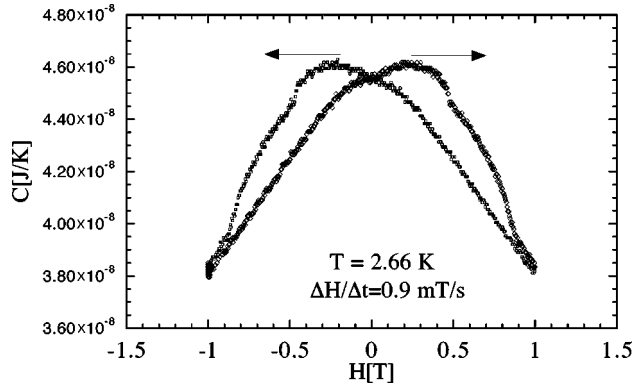

FIG. 10. Total heat capacity of the 20-μg sample vs a magnetic field swept at 0.9 mT/s. The measuring frequency was $\omega = 25$ Hz.

continuities only appear when the applied field is antiparallel to the initial magnetization and why their shape strongly depends on the sweeping rate.

The time-dependent magnetic heat capacity $C(t)$ can be calculated with Eq. (A11). The coefficients p_m are given by Eq. (14), where p^+ and p^- obey the relaxation law (19), but are unknown. τ is, in this case, the effective magnetization relaxation time (thermal activation+tunneling). The interest of these nonequilibrium measurements is, first, that they can be directly compared to magnetization curves and second, they could permit, in certain cases, the measurement of the time derivative $(\partial/\partial t)p^m(t)$, thus yielding information on the still unknown spin-phonon interaction of the system.

IV. TEMPERATURE MEASUREMENTS

A major problem in the study of macroscopic quantum coherence effects is to evaluate the influence of thermal fluctuations on measurements. Thermal activation is a concurrent effect to tunneling of magnetization; it is thus difficult to distinguish one from the other.

In a previous work[13] we presented temperature measurements of the samples as a function of an applied magnetic field ($T[H]$) (Figs. 5 and 6). We found that the Mn_{12} crystals emitted heat pulses at discrete field values that were multiples of $H = D/(g\mu_B) \simeq 0.4$ T. The influence of the temperature of the base line and the sweeping rate were investigated. The field was ramped from a large negative value (saturated sample) to a large positive one at a relatively high rate of 5–17 mT/s. The heat capacity of the sample holder was at least one order of magnitude smaller than the heat capacity of the sample, so we can consider the measured temperature to be the real sample temperature. The curves traced in Figs. 5 and 6 of Ref. 13 for two different samples show a different character, in spite of the fact that the mass is the only difference between the two crystals.

A. Total magnetization reversal

Figure 5 of our previous work[13] shows the heat emission of the 20-μg sample at different temperatures. Close to 3 K the main peak appears at 0.4 T. At lower temperatures this peak decreases, and finally disappears, while the 0.8-T peak gains in amplitude. At 2.2 K the latter peak has also disappeared. In all cases a small peak is found at zero field. It is due to the sample holder, not to the sample. The heat emission can be understood in the framework of the present double-well model. The system is always in the unilateral regime. When the sample is saturated in a high magnetic field a great majority of spins are in the ground state $m = 10$. The field is ramped from the starting value (-1 T) up to $H = D/(g\mu_B) \simeq 0.4$ T without any significant temperature change. At this field value the $m > 0$ and $m < 0$ levels become degenerate and a transfer of spins from the $m > 0$ well to the $m < 0$ occurs by thermally activated tunneling between degenerate levels. The observed heat emission is due to the relaxation of tunneled spins to the ground state. Their energy is transmitted to the phonon bath. The temperature of the sample goes up to ~ 6 K during the heat emission, a temperature at which the relaxation time of magnetization becomes smaller than 1 ms. At higher magnetic fields no further heat emissions occur, suggesting that all spins have already flipped.

B. Partial magnetization reversal

The peaks in Fig. 6 show a different behavior. The weakness of the heat emission suggests that only small regions of the crystal or a certain amount of single independent macrospins reverse. When the temperature is decreased, new peaks at higher magnetic fields become visible and low-field ones vanish. The shape and position of the peaks depend on the relaxation time of magnetization τ and its relation to the sweeping rate of the magnetic field. If the time spent at a crossing of levels $[H = nD/(g\mu_B)]$ is small compared with τ, only a small number of spins change to the other well. At the next level crossing $g\mu_B H = (n+1)D$, the anisotropy is lower, so that τ is smaller, tunneling is faster, and the specific peak is higher. Sooner or later a complete magnetization reversal is achieved. The reasons for the different behavior compared to the 20-μg crystal are (i) the shorter thermal relaxation time to the bath of the 1-μg crystal ($\tau_{th} = C/K$ where the thermal link K, defined by the sample holder, is the same for both samples) and (ii) the more favorable ratio of surface to volume of the smaller sample. In other words, the 1-μg sample dissipates the emitted heat faster, so that the crystal has no time to globally increase its temperature. The very different behavior of these otherwise identical samples outlines the great importance of thermal effects in magnetization relaxation. Our measurements qualitatively reproduce the magnetization measurements of a Mn_{12}-acetate single crystal performed by Thomas *et al.*[29] and, in addition, they provide important additional information, the real temperature of the crystal.

C. Thermal amplification of spin tunneling

Paulsen and Park reported[9] nonreproducible complete magnetization reversals of Mn_{12}-acetate crystals measured at very low temperatures ($T \ll 1$ K). According to the authors, the reversals occurred at random magnetic-field values and they might be caused by avalanches of spin flips: A spin tunnels and relaxes to the ground state while emitting heat. The temperature of the neighbor clusters is raised by the heat pulse above the blocking temperature, greatly increasing the probability that they will flip. In turn they heat their neighbors and so on, until all spins have turned over. Paulsen and

Park had a sample that was very well thermally coupled to the bath, so the low thermal conductivity of the Mn_{12} acetate at low temperatures was responsible for local overheating. It seems likely that the energy liberated by tunneling spins triggers small avalanches of spin flips in their neighborhood. This effect would strongly thermally enhance the tunneling of spins, though total magnetization reversal may not happen, as in Fig. 6 of our previous work.[13] The avalanches would stop as soon as the degeneracy of opposite levels is lifted. To conclude whether microavalanches triggered by magnetization tunneling are relevant or not, the thermal conductivity of Mn_{12} acetate must be measured and the spin-lattice interaction must be known.

D. Shift of peaks with temperature

The 0.8-T peak of the $T(H)$ curves of Fig. 5 of our previous work[13] shifts slightly to higher fields with decreasing temperature. Two possible effects could explain this shift.

(1) The influence of magnetization on the local field of the sample. The real magnetic field experienced by every spin of the crystal is, to a first approximation, $B=\mu_0(H-nM+M)$, where H is the applied magnetic field, n the demagnetizing factor, and M the magnetization of the sample. M varies with temperature. Hernández *et al.*[16] explain in this way a shift of their dM/dH peaks that seems to be of the same nature.

(2) Barra *et al.*[17] have demonstrated by means of electron paramagnetic resonance measurements the existence of a fourth-order magnetic anisotropy term in the Hamiltonian of the Mn_{12}-acetate systems. The fourth-order term introduces an asymmetry into the Hamiltonian so that the levels of one well do not all match exactly at the same magnetic-field value with the corresponding levels of the opposite well. The population of levels varies with temperature, so different levels can dominate at different temperatures and in consequence the main heat emission happens at slightly different fields. This effect is especially remarkable at high-field crossings.

Further measurements will allow the evaluation of the importance of these mechanisms and help to discern the nature of the higher-order terms of the Hamiltonian.

V. CONCLUSION

A study of the frequency-dependent heat capacity of a Mn_{12}-acetate magnetic double-well system has been presented. A theory has been developed, which relates the experimentally measured, frequency-dependent specific heat to the bilateral and unilateral specific heats (easily calculated from electron paramagnetic resonance data) and the magnetic relaxation time τ. The results reproduce the anomalies of τ as a function of the magnetic field although they do not provide a very precise value of τ. Consideration of higher-order terms in Eq. (1) (for instance, the fourth-order terms in Ref. 17) might increase the accuracy.

Measurements of heat emission confirm that the thermal coupling between bath and sample plays a major role in the magnetization reversal. We point out the importance of parameters such as the thermal conductivity and the heat capacity of the sample in the magnetization reversal of molecular magnets. We conclude that the magnetization tunneling in Mn_{12} acetate was, in our case, enhanced by a thermal amplification effect caused by the weakness of the thermal link to the bath and we suggest that tunneled spins could generally act as a trigger of microavalanches of reversed spins.

ACKNOWLEDGMENTS

The authors want to thank F. Bartolomé, M. Giroud, M. Novak, and R. Sessoli for useful discussions. We also thank M. Hunt for useful help.

APPENDIX: DYNAMICAL SPECIFIC HEAT

In this appendix we derive formula (24). Replacing $T=1/(k_B\beta)$ by Eqs. (2) and (3) in expression (17) of p_{eq}^{+}, one obtains

$$p_{eq}^{+}(t)=p_0^{+}+\delta p_0^{+}\cos(\omega t), \tag{A1}$$

where p_0^{+} is defined by Eq. (22) and, if ψ_m is chosen independent of T,

$$\delta p_0^{+}=\left(\frac{dp_{eq}^{+}}{dT}\right)_{T=T_0}\qquad \delta T_0=p_0'^{+}\,\delta T_0, \tag{A2}$$

$$\begin{aligned}=k_B\beta_0^2\frac{\sum_m E_m\exp(-\beta_0E_m)(1+\psi_m)/2}{\sum_m\exp(-\beta_0E_m)}\\ -k_B\beta_0^2\frac{\sum_m\exp(-\beta_0E_m)(1+\psi_m)/2}{\sum_m\exp(-\beta_0E_m)}\\ \times\frac{\sum_m E_m\exp(-\beta_0E_m)}{\sum_m\exp(-\beta_0E_m)}.\end{aligned} \tag{A3}$$

Quantities p_0^{-} and $p_0'^{-}$ can be defined in a similar way, and are, respectively, equal to $p_0^{-}=1-p_0^{+}$ and $p_0'^{-}=-p_0'^{+}$.

Insertion of Eq. (A1) in Eq. (19) yields Eq. (20).

Inserting Eq. (20) into Eq. (16) one obtains for weak temperature modulations

$$\begin{aligned}U(t)&=p^{-}(t)U^{-}[T(t)]+p^{+}(t)U^{+}[T(t)]\\ &=p_0^{-}U^{-}[T(t)]+p_0^{+}U^{+}[T(t)]\\ &\quad+\frac{1}{\sqrt{1+\omega^2\tau^2}}[\delta p_0^{-}U^{-}(T_0)+\delta p_0^{+}U^{+}(T_0)]\\ &\quad\times\cos(\omega t-\alpha),\end{aligned} \tag{A4}$$

where

$$U^{\pm}(T)=\frac{1}{z^{\pm}}\sum_m E_m\exp(-\beta E_m)\,\frac{1\pm\psi_m}{2}. \tag{A5}$$

Relation (A4) can be written as

$$U(t)=p_0^- U^-(T_0)+p_0^+ U^+(T_0)+\delta U(t) \tag{A6}$$

with

$$\delta U(t)=[p_0^- C^-(T_0)+p_0^+ C^+(T_0)]\delta T_0 \cos\,\omega t + \frac{1}{\sqrt{1+\omega^2\tau^2}}[\delta p_0^- U^-(T_0)+\delta p_0^+ U^+(T_0)] \times \cos(\omega t-\alpha), \tag{A7}$$

where, if ψ_m is independent of T,

$$C^{\pm}(T)=\frac{1}{k_B T^2}\sum_m E_m^2 \exp(-\beta E_m)\,\frac{1\pm\psi_m}{2z^{\pm}} - \frac{1}{k_B T^2}[U^{\pm}(T)]^2. \tag{A8}$$

Formula (A7) can be written in the form (23) where

$$\tan\,\varphi=\frac{[p_0'^- U^-(T_0)+p_0'^+ U^+(T_0)]\sin\,\alpha/\sqrt{1+\omega^2\tau^2}}{p_0^- C^-(T_0)+p_0^+ C^+(T_0)+[p_0'^- U^-(T_0)+p_0'^+ U^+(T_0)]\cos\,\alpha/\sqrt{1+\omega^2\tau^2}} \tag{A9}$$

and

$$|C(\omega)|^2=\left\{p_0^- C^-(T_0)+p_0^+ C^+(T_0)+\frac{p_0'^- U^-(T_0)+p_0'^+ U^+(T_0)}{\sqrt{1+\omega^2\tau^2}}\cos\,\alpha\right\}^2+\frac{[p_0'^- U^-(T_0)+p_0'^+ U^+(T_0)]^2}{1+\omega^2\tau^2}\sin^2\,\alpha.$$

Using relations $\cos\,\alpha=1/\sqrt{1+\omega^2\tau^2}$ and $\sin\,\alpha=\omega\tau/\sqrt{1+\omega^2\tau^2}$, which result from Eq. (21), the previous formula reads

$$C^2(\omega)=C_{uni}^2+[C_{bi}^2-C_{uni}^2]\cos^2\alpha, \tag{A10}$$

which reduces to Eq. (24).

C_{uni} is given by

$$C_{uni}=p_0^- C^-(T_0)+p_0^+ C^+(T_0), \tag{A11}$$

while

$$C_{bi}=p_0^- C^-(T_0)+p_0^+ C^+(T_0)+p_0'^- U^-(T_0)+p_0'^+ U^+(T_0). \tag{A12}$$

For low temperatures and small magnetic fields we obtain approximately

$$C_{bi}=k_B\beta^2\left(\frac{1}{z}\sum_m E_m^2\exp(-\beta E_m) - \left[\frac{1}{z}\sum_m E_m\exp(-\beta E_m)\right]^2\right). \tag{A13}$$

*Electronic address: fominaya@labs.polycnrs-gre.fr

[1] *Quantum Tunneling of Magnetization*, edited by L. Gunther and B. Barbara (Kluwer, Dordrecht, 1995), pp. 171–188.

[2] F. Hartmann-Boutron, P. Politi, and J. Villain, Int. J. Mod. Phys. B **10**, 2577 (1996).

[3] D. D. Awschalom and D. P. DiVincenzo. Phys. Today **48** (4), 43 (1995).

[4] W. Wernsdorfer, K. Hasselbach, B. Barbara, D. Mailly, A. Benoit, L. Thomas, and G. Suran, J. Magn. Magn. Mater. **140-144**, 389 (1995).

[5] T. Lis, Acta Crystallogr., Sect. B: Struct. Crystallogr. Cryst. Chem. **B36**, 2042 (1980).

[6] B. Schwarzschild, Phys. Today **50**, (1) 17 (1997).

[7] M. Hennion, L. Pardi, I. Mirebeau, E. Suard, R. Sessoli, and A. Caneschi, Phys. Rev. B **56**, 8819 (1997).

[8] M. A. Novak and R. Sessoli, in *Quantum Tunneling of Magnetization*, edited by L. Gunther and B. Barbara (Kluwer, Dordrecht, 1995), pp. 171–188.

[9] C. Paulsen and J. G. Park. *Quantum Tunneling of Magnetization* (Ref. 1), pp. 189–207.

[10] B. Barbara, W. Wernsdorfer, L. C. Sampaio, J. G. Park, C. Paulsen, M. A. Novak, R. Ferré, D. Mailly, R. Sessoli, A. Caneschi, K. Hasselbach, A. Benoit, and L. Thomas, J. Magn. Magn. Mater. **140-144**, 1825 (1994).

[11] M. A. Novak, R. Sessoli, A. Caneschi, and D. Gatteschi, J. Magn. Magn. Mater. **146**, 211 (1995).

[12] J. R. Friedman, M. P. Sarachik, J. Tejada, and R. Ziolo, Phys. Rev. Lett. **76**, 3830 (1996).

[13] F. Fominaya, J. Villain, Ph. Gandit, and J. Chaussy, Phys. Rev. Lett. **79**, 1126 (1997).

[14] P. Politi, A. Rettori, F. Hartmann-Boutron, and J. Villain, Phys. Rev. Lett. **75**, 537 (1995).

[15] J. Villain, F. Hartmann-Boutron, R. Sessoli, and A. Rettori, Europhys. Lett. **27**, 159 (1994).

[16] J. M. Hernández, X. X. Zhang, F. Luis, J. Tejada, J. R. Friedman, M. P. Sarachik, and R. Ziolo, Phys. Rev. B **55**, 5858 (1997).

[17] A. L. Barra, D. Gatteschi, and R. Sessoli, Phys. Rev. B **56**, 8192 (1997).

[18] F. Fominaya, T. Fournier, P. Gandit, and J. Chaussy, Rev. Sci. Instrum. **68**, 4191 (1997).

[19] M. Meissner and K. Spitzmann, Phys. Rev. Lett. **46**, 265 (1981).

[20] N. O. Birge and S. R. Nagel, Phys. Rev. Lett. **54**, 2674 (1985).

[21] P. F. Sullivan and G. Seidel, Phys. Rev. **173**, 679 (1968).

[22] E. Schrödinger, *Statistical Thermodynamics* (Cambridge University Press, Cambridge, 1960), Chap. 5.
[23] A. Fort, A. Rettori, J. Villain, D. Gatteschi, and R. Sessoli, Phys. Rev. Lett. **80**, 612 (1998).
[24] J. F. Fernández, F. Luis, and J. Bartolomé, Phys. Rev. Lett. **80**, 5659 (1998).
[25] F. Luis, J. Bartolomé, and J. F. Fernández, Phys. Rev. B **57**, 505 (1998).
[26] Charles Kittel, *Introduction to Solid State Physics*, 6th ed. (Wiley, New York, 1984).
[27] R. Sessoli, D. Gatteschi, A. Caneschi, and M. A. Novak, Nature (London) **365**, 141 (1993).
[28] J. M. Hernández, X. X. Zhang, F. Luis, J. Bartolomé, J. Tejada, and R. Ziolo, Europhys. Lett. **35**, 301 (1996).
[29] L. Thomas, F. Lionti, R. Ballou, D. Gatteschi, R. Sessoli, and B. Barbara, Nature (London) **383**, 145 (1996).